The Astrophysical Journal, 904:46 (9pp), 2020 November 20 https://doi.org/10.3847/1538-4357/abbda4

Analytical and Numerical Studies of Central Galactic Outflows Powered by Tidal Disruption Events: A Model for the Fermi Bubbles?

C. M. Ko[1,2], D. Breitschwerdt[3], D. O. Chernyshov[4,5], H. Cheng[1], L. Dai[6,7], and V. A. Dogiel[4]
[1] Institute of Astronomy, National Central University, Zhongli Dist., Taoyuan City, Taiwan (R.O.C.); cmko@astro.ncu.edu.tw
[2] Department of Physics and Center for Complex Systems, National Central University, Zhongli Dist., Taoyuan City, Taiwan (R.O.C.)
[3] Zentrum für Astronomie und Astrophysik, Technische Universität Berlin, Hardenbergstrasse 36, D-10623 Berlin, Germany
[4] I.E.Tamm Theoretical Physics Division of P.N.Lebedev Institute of Physics, Leninskii pr. 53, 119991 Moscow, Russia; dogiel@td.lpi.ru
[5] Moscow Institute of Physics and Technology (State University), 9, Institutsky lane, Dolgoprudny 141707, Russia
[6] Department of Physics, The University of Hong Kong, Pokfulam Road, Hong Kong
[7] DARK Cosmology Centre, Niels Bohr Institute, University of Copenhagen, Juliane Maries Vej 30, DK-2100 Copenhagen, Denmark
Received 2019 April 18; revised 2020 August 14; accepted 2020 September 30; published 2020 November 20

Abstract

Capture and tidal disruption of stars by the supermassive black hole in the Galactic center (GC) should occur regularly. The energy released and dissipated by these processes will affect both the ambient environment of the GC and the Galactic halo. The single star of a super-Eddington eruption generates a subsonic outflow with an energy release of more than 10^{52} erg, which still is not high enough to push shock heated gas into the halo. Only routine tidal disruption of stars near the GC can provide enough cumulative energy to form and maintain large-scale structures like the Fermi Bubbles. The average rate of disruption events is expected to be $10^{-4} \sim 10^{-5}$ yr^{-1}, providing the average power of energy release from the GC into the halo of $\dot{W} \sim 3 \times 10^{41}$ erg s^{-1}, which is needed to support the Fermi Bubbles. The GC black hole is surrounded by molecular clouds in the disk, but their overall mass and filling factor are too low to significantly stall the shocks from tidal disruption events. The de facto continuous energy injection on timescales of megayears will lead to the propagation of strong shocks in a density stratified Galactic halo and thus create elongated bubble-like features that are symmetric to the Galactic midplane.

Unified Astronomy Thesaurus concepts: Galactic center (565); Interstellar clouds (834); Galactic winds (572); Tidal disruption (1696); Superbubbles (1656); Gamma-rays (637); Cosmic rays (329)

1. Introduction

Two enigmatic gamma-ray features in the Galactic central region, also known as Fermi Bubbles (FBs), were found from Fermi-LAT data (see Dobler et al. 2010; Su et al. 2010; Ackermann et al. 2014). The X-ray and microwave emission around the Galactic center (GC) was detected by Snowden et al. (1997), Bland-Hawthorn & Cohen (2003), and Finkbeiner (2004). Later observations from Planck (see Planck Collaboration IX 2013, and publications in Rubtsov & Zhezher 2018; Jew & Grumitt 2020) showed structures coincided nicely with the FBs.

These features elongated perpendicular to the Galactic plane are seen as a double-bubble structure on the two sides of the plane. The spatial distribution of the emissions from the bubbles shows sharp edges. The surface emissivity is almost uniform inside the bubbles.

These characteristics of gamma-ray and microwave emissions may naturally be interpreted by the radiation of relativistic electrons which are accelerated in situ near the bubble edges (see, e.g., Su et al. 2010; Cheng et al. 2011, 2014, 2015; Mertsch & Sarkar 2011). Crocker & Aharonian (2011) suggested an alternative model of gamma-ray emission from the bubbles, which is produced by collisions of relativistic protons. The reader is referred to Yang et al. (2018) for more details.

We do not consider the problem of particle acceleration in the FBs but concentrate on the origin of their structure and their hydrodynamic evolution. Although the nonthermal and thermal envelopes are of the same origin in general, their structures are defined by different physical processes and their interconnection is indirect.

The ROSAT 1.5 keV image presented a giant structure in the GC, which was seen in thermal X-rays as an open-ended bipolar hour glass (see Bland-Hawthorn & Cohen 2003). This phenomenon required a central event with energetics of about 10^{55} erg whose activity had a timescale of $10 \sim 15$ Myr.

Central galactic outflows have been observed in several galaxies. For example, a structure similar to the FBs was reported recently in NGC 3079 in both nonthermal hard X-rays (Chandra) and in nonthermal radio continuum (JVLA) (Li et al. 2019). The hard X-ray feature has a cone shape with a weak cap at the top with a diameter of ∼1.1 kpc. The authors have found evidence for a significant thermal component above 1 keV, and also argue that cosmic-ray electrons have to be accelerated in situ by shocks. Since most of the data, from gamma to X-rays to radio have been collected for our own galaxy, we will focus here on the so-called FBs.

The origin of energy release at the GC is still an open question. One possibility is that the initial energy release at the GC is a result of accretion onto the central supermassive black hole (SMBH) with a mass of $\sim 4.3 \times 10^6 M_\odot$, which is identified with the source Sgr A* (see Gillessen et al. 2009). The total energy needed to generate large Galactic outflows is assumed to be in the range from 10^{53} to 10^{56} erg (see Bland-Hawthorn & Cohen 2003; Su et al. 2010; Akita et al. 2018; Keshet & Gurwich 2018) if the initial energy release occurred close to the GC in the past.

Several models of the FBs involve a gas outflow from Sgr A* after a huge energy release at the GC ($\sim 10^{55}$–10^{56} erg). For example, Zubovas et al. (2011) and Zubovas & Nayakshin (2012; see also Nayakshin & Zubovas 2018) suggested that a giant molecular cloud of mass $\sim 10^5 M_\odot$ was captured by the

SMBH in the GC about 1 Myr ago. A simplified model is described by a shock front of a relatively short single burst propagating through the halo of a uniform density.

Mou et al. (2014) assumed an alternative scenario, in which the mass accretion rate of hot gas flow onto Sgr A* was $10^3 \sim 10^4$ times higher in the past. Its activity lasted for 10^7 yr and ceased about 2×10^5 yr ago. During these 10^7 yr the bubble propagated several kiloparsecs out into the halo, driven by winds launched from the accretion flow onto Sgr A*. Similar models of ongoing energy release in the GC were suggested for the interpretation of the local GC $e^{\pm}$ annihilation line (Cheng et al. 2006, 2007; Totani 2006).

Guo & Mathews (2012), Guo et al. (2012), and Zhang & Guo (2020; see also Yang et al. 2012) developed a model of the bubble at the GC with recent active galactic nucleus (AGN) jet activity, occurring $1 \sim 3$ Myr ago. Cosmic-ray effects were included in their MHD model. The FB evolution is described by a system of nonlinear hydrodynamic equations, similar to Drury & Völk (1981) for CR acceleration at shocks or to Breitschwerdt et al. (1991) for wind escape from the Galactic wind. The active period of energy release at the GC is $0.1 \sim 0.5$ Myr. The total energy release was estimated as $10^{55} \sim 10^{57}$ erg. The model of the envelope with arbitrary/undefined parameters describes, nevertheless, a proper structure of the FBs.

We notice that sharp edges of the FBs and the uniform surface emissivity inside the bubble can be interpreted as a result of acceleration of relativistic electrons by turbulence and shocks inside and near the boundary of FBs (see Cheng et al. 2011, 2014, 2015).

An alternative energy release was suggested in the GC by star formation activity over about 10^7 yr (see, e.g., Carretti et al. 2013; Nakashima et al. 2018; Zhang et al. 2020). In principle this process may also produce energy outflow from the star formation region in the CMZ (central molecular zone, a sheet-like structure surrounding the GC). We note that star formation activity near the GC is still under debate. Some studies of star formation regions near the GC indicated that star formation activity is suppressed, and it may not play a significant role in comparison with processes in starburst galaxies (see, e.g., Kauffmann 2017). On the other hand, there are indications that there might be increased star formation activities at GC in recent times (Genzel et al. 2010; Nogueras-Lara et al. 2020; although not comparable to starburst galaxies).

Recent X-ray observations in the direction of the constellation Draco (X-ray source Swift J1644+57) found a more moderate energy release. The peak luminosity was detected to be $\sim 10^{48}$ erg s^{-1}, and the total energy release was estimated to be 3×10^{53} erg (Burrows et al. 2011). Another example of a huge energy release was presented in Donato et al. (2014), who interpreted a flare in the cluster A1795 as a stellar disruption with an energy release of about 1.7×10^{52} erg by a black hole with a mass of $\sim 3 \times 10^5\, M_\odot$. Li et al. (2020) presented results of monitoring observations of a stellar tidal disruption event (TDE) by a supermassive black hole ($\sim 5 \times 10^7\ M_\odot$) in NGC5092. Over a period of 13 yr the overall X-ray luminosity was estimated to be $\sim 1.5 \times 10^{43}$ erg s^{-1}.

Cheng et al. (2011, 2012) speculated about the origin of the FBs as the result of routine stellar TDEs by the central black hole. The expected energy release produced by accretion processes in the GC is about $\gtrsim 10^{52}$ erg, depending on the mass of the captured stars close to Sgr A. Less than 0.04 pc from it are about 35 low-mass stars ($1 \sim 3M_\odot$) and about 10 massive stars ($3 \sim 15M_\odot$), see, e.g., Alexander & Livio (2004), Alexander (2005), and Genzel et al. (2010). The expected rate of stellar capture per galaxy from theoretical calculation is $\sim 2 \times 0^{-4}$ yr^{-1} (Magorrian & Tremaine 1999; Wang & Merritt 2004; Generozov et al. 2018).

Observational evidence of energy release from Sgr A* was recently found. The estimates are very crude, but they give a qualitative understanding of processes involved. X-ray and radio observations showed a pair of lobes on a scale of about 15 pc, located above and below the Galactic plane, surrounding the GC (Morris et al. 2003; Zhao et al. 2016). They are filled with plasma at temperature $0.7 \sim 1$ keV. More recently, using XMM and Chandra, Ponti et al. (2019) obtained a detailed X-ray map of a region nearby Sgr A*. They found two elongated structures extending above and below the GC, which are called the northern and southern Galactic center chimneys. These quasi-linear structures are about 160 pc in length and have sharp edges. Their thermal energy content is about 4×10^{52} erg. The gas density within the chimneys decreases with latitude from about 0.2 cm^{-3} at 30 pc to about 0.1 cm^{-3} at 160 pc. The authors suggested that the chimneys connect the regions around the GC to the FBs. An X-ray plume of size $\sim 1^\circ$ observed by Suzaku is interpreted as a magnetized hot gas outflow from the GC (Nakashima et al. 2019).

Using the MeerKAT, Heywood et al. (2019) found a pair of radio bubbles at the GC. The structure is seen as a pair of bounded bipolar bubbles spanning 140 pc $\times$ 430 pc across the Galactic plane. The radio emission is consistent with synchrotron radiation. The total energy in the radio bubbles is estimated to be 7×10^{52} erg. The energy is much less than the total energy content of the FBs, but the authors indicated that the radio bubbles may be an example of a series of similar events (and possibly combined with steadier outflows), where cumulative effects may be responsible for the radio, X-ray, and gamma-ray structures that connect the GC to the halo.

These observations provide evidence of energetic outbursts from the surroundings of the GC, which propagate preferentially perpendicular to the Galactic plane, and, in combined action, may produce the necessary amount of energy to generate the FBs or similar structures.

The paper is organized as follows. In Section 2 we discuss the energetics of TDEs at the GC. In Section 3 we argue how the energy from the TDEs propagate through the Galactic disk to the halo. Two models for the density distribution of the halo are described. In Section 4 we present analytical solutions for the shock propagation in the halo of the two halo models. In Section 5 we perform numerical calculations for the development of the bubbles in the two halo models. Section 6 provides a summary.

2. Plasma Outflow Generated by Stellar Disruptions and Subsequent Shock Formation

In the following we adopt the hypothesis that cumulative routine stellar disruptions by the SMBH are responsible for the formation of the FBs or similar structures. X-ray observations of jetted TDEs Sw 1644 (Kara et al. 2016) and non-jetted TDEs (Lin et al. 2017) can be interpreted as fast outflows from super-Eddington accretion. This process was analyzed in numerical simulations by Dai et al. (2018). They showed that the accretion energy is mainly carried away by the following channels: (1) radiation with efficiency of $\eta_{\rm rad} \approx 3\%$, (2) jet with $\eta_{\rm jet} \approx 20\%$, and (3) outflow with $\eta_{\rm of} \approx 20\%$ (where η is the ratio of the energy conversion rate to the

rest mass accretion rate $\dot{M}c^2$). Also, the outflow has a speed of several tenths of the speed of light, c, for most inclination angles. The specific values of the efficiencies and the outflow speed depend on parameters such as the mass, the spin of the black hole, and the accretion rate. However, most of the current simulations of super-Eddington accretion with parameter settings have given consistent results (e.g., Jiang et al. 2014; Sądowski & Narayan 2016). Therefore, we adopt that, in all TDEs, outflows with speeds of several tenths of c are produced and they carry away up to 10% of the accretion energy. Such fast outflows provide the largest impact on the surrounding matter since they can carry a lot of matter moving with nonrelativistic speed. Also, it is likely that only a small fraction of TDEs can produce jets.

Given the average mass of outbound matter, which is approximately $0.5M_{\odot}$ for a TDE of a solar mass star, one can estimate the total energy of the outflow as $\sim 10^{52}$–10^{53} erg. With these input parameters (outflow velocity $v_0 \approx 0.1c$–$0.3c$, total energy $W \approx 10^{52}$–10^{53} erg), we intend to describe the outflow into the surrounding medium of the black hole. In terms of total efficiency, it accounts for up to $1 \sim 10\%$ of the total rest mass energy of the disrupted star.

3. Shock Propagation through the Galaxy

3.1. Shock Propagation through the Galactic Disk

A sudden (sporadic) energy release by a TDE in the GC generates a cavity with a shock that expands into the local ambient medium. This process is analogous to a supernova (SN) explosion and the subsequent evolution of the supernova remnant (SNR). The model of SNR shock propagation in a low pressure environment was developed by, e.g., Cox (1972) and Blondin et al. (1998). At the initial phase the expanding cavity can be described by the Sedov solution (Sedov 1959) when the total energy released is almost confined within the envelope. In a later phase the solution differs from the similarity one due to radiative cooling in the envelope, and energy losses become important. The pressure behind the neutral shell drops significantly, and the envelope expands until the pressure of the cavity reduces to the ambient pressure of the interstellar medium (ISM), and the shell merges with the ISM.

The radius and time of the transition from the Sedov phase to the radiative phase can be estimated as

$$R_s \approx 19.1 \times W_{51}^{5/17} n_{\rm H}^{-7/17} \ {\rm pc}, \quad (1)$$

$$t_s \approx 2.9 \times 10^4 \times W_{51}^{4/17} \, n_{\rm H}^{-9/17} \ {\rm yr}, \quad (2)$$

where W_{51} is the energy release of TDE in units of 10^{51} erg and $n_{\rm H}$ in ${\rm cm}^{-3}$.

The question is whether the envelope pierces through the Galactic disk without significant braking, so that the shock can pick up speed in a decreasing halo density environment. The ISM in the CMZ is very complex. The gas density in the ambient medium of the GC is not well known and quite difficult to assess. A standard model of the gas distribution in the CMZ was presented by Ferrière (2001, 2012) and Ferrière et al. (2007), where about 80% of the volume consists of two phases: a hot coronal component at a temperature of about $10^5 \sim 10^6$ K with an average density of about $\sim 10^{-3}$ ${\rm cm}^{-3}$ and a warm ionized medium with a temperature of $T \sim 10^4$ K and a density of $0.1 \sim 1$ ${\rm cm}^{-3}$. For a single explosion (i.e., a burst of energy) in the GC with an energy release of $E_0 \sim 10^{52}$–10^{53} erg, the envelope still retains a fair amount of the blast wave energy in the Sedov phase for a single event, when the Sedov radius $R_{\rm ad}$ in the GC is about 100 pc, i.e., comparable to or larger than the thick Galactic gas disk. The cavity can then penetrate into the halo within its Sedov phase, even for a single explosion of moderate energy release, and the radiation losses can be neglected. One should also keep in mind that once gas has been pushed aside by an explosion, a hole in the gas layer considerably alleviates the break-out of successive explosions. The "self-healing" time of these holes is of the order of the cooling time and the subsequent loss of pressure, plus the sound crossing time in which denser and cooler material flows in, which is of the order of $10^6 \sim 10^7$ yr, much longer than the time interval for the next event to occur.

Recent observations of molecular lines in the directions of molecular clouds found an intermittent gas with average density of about 10^4 ${\rm cm}^{-3}$ (Mills 2017; Mills et al. 2018). However, the volume filling factor of molecular clouds in the CMZ is much less than 0.1.

Oka et al. (2019) suggested a new interpretation of the CMZ, unlike the standard model of the ISM in the GC. The volume of the CMZ is dominated by the diffuse molecular gas with a temperature of $T \sim 200$ K and a density of $n \sim 50$ ${\rm cm}^{-3}$. The filling factor for dense gas with $n > 10^4$ ${\rm cm}^{-3}$ should therefore be much less than 0.1. The ultra hot X-ray-emitting plasma with a temperature of $T \sim 10^8$ K, which some thought to dominate the CMZ, does not coexist with the diffuse molecular gas and is thus not spread over extended regions. The observed diffuse X-ray emission in the CMZ must be due to unresolved point sources and to scattering by interstellar atoms and molecules. If this is true, the Sedov radius in the CMZ is about 15 pc for a single explosion of 10^{53} erg. The cavity is unable to penetrate through the Galactic disk ($\sim$100 pc), and its energy is dumped there. The time of transition from the Sedov phase to the radiative phase for $n_{\rm H} = 50$ ${\rm cm}^{-3}$ is about $t_s \simeq 1 \sim 2 \times 10^4$ yr (see Equation (2)). The energy is transformed into radiation completely for the time $t_E \sim 10^7$ yr within the radiative radius $R_E \sim 400$ pc (see McKee & Ostriker 1977), i.e., a significant fraction of the energy release is lost in the disk.

Alternatively, if another TDE occurs within the time $t < t_s$ in the GC, then the cumulative effect provides a more extended Sedov radius than that of a single event. The rate of the average TDEs of stars is about 10^{-4} ${\rm yr}^{-1}$ (Syer & Ulmer 1999), and the total average power in the GC can be estimated as $\dot{W} \lesssim 3 \times 10^{41}$ erg ${\rm s}^{-1}$. This scenario holds, when routinely occurring TDEs punch through the disk and deposit energy into the halo. However, we point out that the epoch of routine TDEs at the GC cannot exist forever. It depends on the activities at the Galactic central regions, which are highly variable (see, e.g., Melia & Falcke 2001; Genzel et al. 2010; Nogueras-Lara et al. 2020).

This type of energy release is similar to processes of stellar winds described in Avedisova (1972), McCray et al. (1975), and Weaver et al. (1977). The hydrodynamic structure of the expanding cavity can be described by a Sedov solution for multi-captures. The end of the adiabatic phase occurs at radius and time (Avedisova 1972),

$$R_{\rm ad} \approx 1.93 \times \dot{W}_{36}^{2/5} n_{\rm H}^{-3/5} \ {\rm pc}, \quad (3)$$

$$t_{\rm ad} \approx 7.5 \times 10^3 \times \dot{W}_{36}^{1/3} n_{\rm H}^{2/3} \ {\rm yr}, \quad (4)$$

where $\dot{W}$ is the power input in 10^{36} erg ${\rm s}^{-1}$. Even for $n_{\rm H} \sim 50$ ${\rm cm}^{-3}$ and a power in the GC of about $\dot{W} \lesssim 3 \times 10^{41}$ erg ${\rm s}^{-1}$

the Sedov radius in the disk is 70 pc. The thickness of CMZ is a few tens of parsecs (Morris & Serabyn 1996), and for these parameters of the disk the envelope can penetrate freely into the halo, even for the case of multi-captures.

3.2. Gas Distribution in the Halo

As in the disk, the gas distribution in the halo is not very reliable. For instance, Cordes et al. (1991) and Biswas & Gupta (2018) assume that the plasma density in the Galactic halo drops exponentially with height z above the Galactic plane,

$$n(z) = n_0 \exp\left(-\frac{z}{z_0}\right), \tag{5}$$

where n_0 is the gas number density at $z = 0$ and z_0 is the density scale height. Nordgren et al. (1992) estimated the density of free electrons above the plane as $n_0 = 0.033\,\mathrm{cm}^{-3}$ and the characteristic scale of the electron distribution there as $H = 0.53$–0.84 kpc. Similarly, Gaensler et al. (2008) derived the warm plasma distribution ($\sim 10^4$ K) above the Galactic disk ($\lesssim$2 kpc with the average density $\sim 0.014\,\mathrm{cm}^{-3}$) from pulsar dispersion measures and Hα diffuse emission.

The gas distribution of the hot gas in the halo with temperature $T \sim 10^6$ K was derived from the Suzaku observation (Nakashima et al. 2018). The distribution can be expressed as a disk-like density distribution

$$n(R, z) = n_0 \exp\left(-\frac{R}{R_0}\right)\exp\left(-\frac{z}{z_0}\right), \tag{6}$$

with $n_0 \simeq 4 \times 10^{-3}\,\mathrm{cm}^{-3}$, the scale height $z_0 \simeq 2$ kpc, and the radial scale length $R_0 \simeq 7$ kpc.

The first indication on the X-ray structure was found by Snowden et al. (1997) from ROSAT, which was seen as a bulge of hot gas similar to a cylinder with an exponential fall-off of density with height above the plane. The cylinder has a radial extent around 5.6 kpc, and the scale height of 1.9 kpc with electron density at the base of about $0.0035\,\mathrm{cm}^{-3}$ and temperature of about 10^6 K. Recent observations by Swift and Suzaku were interpreted as a bubble-in-halo in which two identical bubbles expand within a halo forming a thick uniform shell of swept-up halo gas. Assuming that the 0.3 keV plasma is heated by a shock driven by the bubbles' expansion in the surrounding halo, the corresponding velocity is about 300 km s^{-1} (Kataoka et al. 2015; Tahara et al. 2015).

Miller & Bregman (2013, 2016) derived a so-called β-model of the gas density profile in the halo from the intensity of absorption lines. The diffuse gas density in the Milky Way halo is approximated by a flattened profile

$$n(R, z) = n_0 \left[1 + \left(\frac{R}{R_c}\right)^2 + \left(\frac{z}{z_c}\right)^2\right]^{-3\beta/2}, \tag{7}$$

where $n_0 \simeq 0.5\,\mathrm{cm}^{-3}$ is the core density, R_c and z_c represent the effective core radial and vertical distance, and the exponent β is the slope of the profile. For the GC gas distribution, we can use $R = 0$, so that for $z \gg z_c$ the distribution simplifies to

$$n(z) = n_0 \left(\frac{z_c}{z}\right)^{3\beta}, \tag{8}$$

and $z_c = 0.26$ kpc is used (see Miller & Bregman 2013).

In these publications the authors presented a number of arguments in favor of the β-model (for details, see Miller & Bregman 2013, 2016). It is clear that the exponential model, in comparison to the β-model, would overestimate the ability of shocks to penetrate the Galaxy halo, as well as the distance of shock propagation into the Galactic halo, thus affecting the predicted bubble morphology as well.

4. Analytical Solution for Shock Propagation in Exponential and Power-law Density Profiles of the Galactic Halo

Kompaneets (1960; see also Shapiro 1979, the review of Bisnovatyi-Kogan & Silich 1995, and the monograph of Zel'dovich & Raizer 1967) developed the formalism of strong explosions with energy E when a shock front is propagating through an exponential atmosphere with the density distribution $n(z) = n_0 \exp(-z/z_0)$. He showed in this model that the shock propagates to infinity within a finite time.

Baumgartner & Breitschwerdt (2013) developed an analytical solution of a hydrodynamic model for a shock wave propagation for different energy input rates for single and successive explosions in exponential atmospheres in star-forming regions in the disk. The authors showed that the shock surface accelerates when its velocity is above the sound speed, and that it develops Rayleigh–Taylor instabilities at the top of the envelope. We expect that the shock propagation in a galactic halo with a β-atmosphere differs noticeably from that of an exponential model in star formation regions or TDEs at GC.

Following the Kompaneets formalism (see details in Bisnovatyi-Kogan & Silich 1995), the shock front is described as

$$\left(\frac{\partial r}{\partial y}\right)^2 - \frac{1}{\mathcal{R}(z)}\left[\left(\frac{\partial r}{\partial z}\right)^2 + 1\right] = 0, \tag{9}$$

with a transformed time variable

$$y = \int_0^t \sqrt{\frac{(\gamma^2 - 1)}{2}\frac{2W(t)}{3\rho_0 V(t)}}\, dt, \tag{10}$$

where γ is the ratio of the specific heats, $\rho_0 = n_0\bar{m}$ is the mass density of the background gas, with $\bar{m}$ being the average atomic mass for a given metallicity, $W(t)$ is the energy released by a central source, and $V(t)$ is the current volume of the expanding bubble,

$$V(t) = \pi \int_0^{z_u} r^2(z, t)dz. \tag{11}$$

Here $r(z, t)$ is the radius of the envelope in cylindrical coordinates, and z_u is height of the top of the bubble. $\mathcal{R}(z)$ describes the structure of the atmosphere or halo, e.g., $\rho(z) = \rho_0\mathcal{R}(z)$. In the following we discuss two different structures: (1) $\mathcal{R}(z) = \exp(-z/z_0)$ and (2) $\mathcal{R}(z) = (1 + z/z_c)^{-2}$.

4.1. Exponential Density Profile

For an exponential density profile of the halo, $\mathcal{R}(z) = \exp(-z/z_0)$, the solution to Equation (9) is the classic

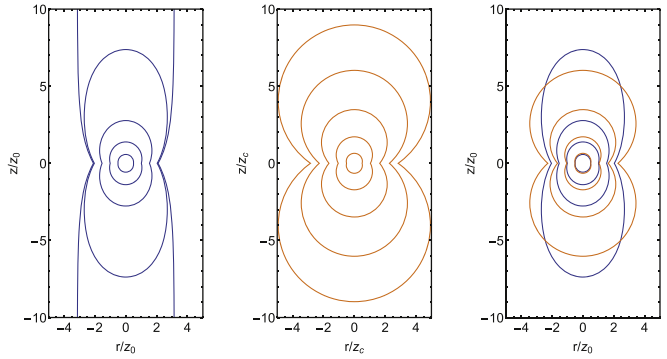

Figure 1. Shock fronts of the bubble for different times y. Left panel: evolution of a bubble in a halo of the exponential density profile. Different contours denote $\tilde{y} = y/z_0 = 0.5, 1.0, 1.5, 1.95, 2.0$. Middle panel: evolution of a bubble in a halo of the power-law density profile. Different contours denote $\tilde{y} = y/z_c = 0.5, 1.0, 1.5, 1.95, 2.3$. Right panel: comparison of bubbles in an exponential halo (in blue) and a power-law halo (in orange) for different times ($\tilde{y} = 0.5, 1.0, 1.5, 1.95$). The two scale heights are set to be the same ($z_0 = z_c$). The bubble in the power-law halo is rounder. The top of the blue bubble catches up with the orange bubble and extends to infinity in finite time.

Kompaneets solution,

$$\cos\left(\frac{r}{2z_0}\right) = \frac{1}{2\sqrt{\mathcal{R}}}\left(\mathcal{R} + 1 - \frac{y^2}{4z_0^2}\right). \tag{12}$$

The top of the bubble is given by

$$\sqrt{\mathcal{R}_u} = \exp\left(-\frac{z_u}{2z_0}\right) = 1 - \frac{y}{2z_0}, \tag{13}$$

and its velocity

$$v_u = \frac{dz_u}{dt} = \exp\left(\frac{z_u}{2z_0}\right)\frac{dy}{dt} = \frac{1}{\sqrt{\mathcal{R}_u}}\frac{dy}{dt}. \tag{14}$$

The left panel of Figure 1 shows the development of the bubble in an exponential halo. Different contours denote the boundary (i.e., the shock) of the bubble at different y (i.e., different times). In an exponential halo, the bubble will developed into a structure asymptotically similar to a cylinder in finite time. As $y \to 2z_0$, the top of the bubble $z_u \to \infty$, and the lateral radius of the bubble $r(z, y \to 2z_0) \to 2z_0 \cos^{-1}(\sqrt{\mathcal{R}}/2)$ (e.g., at the base of the halo $r \to 2\pi z_0/3$, and high up in the halo $r \to \pi z_0$.)

If the shock velocity at any z drops below the sound speed c_s, then it decays and is absorbed in the halo gas. Otherwise, a shock is able to penetrate into the halo with a velocity higher than the sound speed c_s and transfer the energy of the initial central source into the exponential atmosphere. Baumgartner & Breitschwerdt (2013) defined the condition of shock penetration into the exponential atmosphere when the velocity of the shock front is higher than c_s, $v_u > 3c_s$.

For the purpose of illustration, we show in Figure 2 (the left panel) the velocity distribution for the case $z_0 = 0.67$ kpc and $n_0 = 0.03\,\mathrm{cm}^{-3}$, with single input of energy $W = 10^{56}$ erg (thin solid line), $W = 10^{55}$ erg (thick solid line), $W = 10^{54}$ erg (dashed–dotted line), and $W = 10^{53}$ erg (dashed line). The dotted line shows the level $3c_s$ in the halo 3×10^7 cm s^{-1}.

For a single source the energy occupies more and more volume of the exponential atmosphere at $t > 0$, eventually reaching a peak at infinity at finite time. This is an artifact of the Kompaneets' solution, as the shock speed cannot exceed the speed of light. In the end, the structure of a single source disappears as the energy it releases is distributed over an infinite volume. For the parameters in the GC a single star disruption is unable to provide enough energy for the FBs or similar structures, i.e., no more than $10^{52} \sim 10^{53}$ erg (Dai et al. 2018). Our calculations show that an unbelievable single star event with an energy exceeding $W = 10^{54}$ erg is needed to penetrate the disk into the halo.

Alternatively this energy can be supplied by a series of many weaker disruption events with an effective luminosity $\dot{W}$. It follows from Dai et al. (2018) that any star disruption event produces an energy of $10^{52} \sim 10^{53}$ erg with an average rate of star capture of about 10^{-4} yr^{-1}. We show the temporal velocity variations for different values of $\dot{W}$ in the initial development of the structure in the halo in the right panel of Figure 2. We show that the velocity of the envelope exceeds the sound speed if $\dot{W} \gtrsim 10^{40}$ erg s^{-1}. As a result an outflow in the halo can be provided by normal successive star disruptions.

4.2. Power-law Density Profile

We mimic the distribution described by Equations (7) (or (8)) by a power-law density profile, $\mathcal{R}(z) = (1 + z/z_c)^{-3\beta}$. These profiles are similar, in particular, for $z \gg z_c$. If $\beta = 2/3$, the solution to Equation (9) for the power-law density profile is,

$$\left(\frac{r}{z_c}\right)^2 = \sinh^2\left(\frac{y}{z_c}\right) - \left[1 + \frac{z}{z_c} - \cosh\left(\frac{y}{z_c}\right)\right]^2. \tag{15}$$

The top of the bubble is given by

$$\frac{z_u}{z_c} = \cosh\left(\frac{y}{z_c}\right) + \sinh\left(\frac{y}{z_c}\right) - 1, \tag{16}$$

and its velocity

$$v_u = \frac{dz_u}{dt} = \left(1 + \frac{z_u}{z_c}\right)\frac{dy}{dt} = \frac{1}{\sqrt{\mathcal{R}_u}}\frac{dy}{dt}. \tag{17}$$

The middle panel of Figure 1 shows the development of the bubble in a power-law halo. In such a halo, the bubble behaves like an ascending and expanding sphere rising from the base. In contrast to the bubble in an exponential halo, the top of the bubble (or any other part) cannot reach infinity in finite time.

For the single explosion, the lifetime of the envelope is restricted in the halo (even for energy as high as $W = 10^{56}$ erg) and its velocity decreases continuously; see the left panel of Figure 3.

For the case of continuous multi-captures for different values of power, the outflow velocity is shown in the right panel of Figure 3.

We have shown that the velocity of the envelope is constant in the atmosphere and exceeds the sound speed if $\dot{W} \gtrsim 10^{41}$ erg s^{-1}.

When we compare the bubbles in these two density profiles, the shock envelope in a power-law halo becomes broader than in the exponential halo. Therefore the top of the bubble will have traveled a smaller distance from the plane for similar bubble volumes. Apart from that the expansion is quite comparable, and since we expect such a density decrease to hold only for the lower halo, subsequently crossing over to an exponentially decreasing halo at larger distances, the main difference will be a somewhat larger energy input at the base of the halo in order to compensate for this effect.

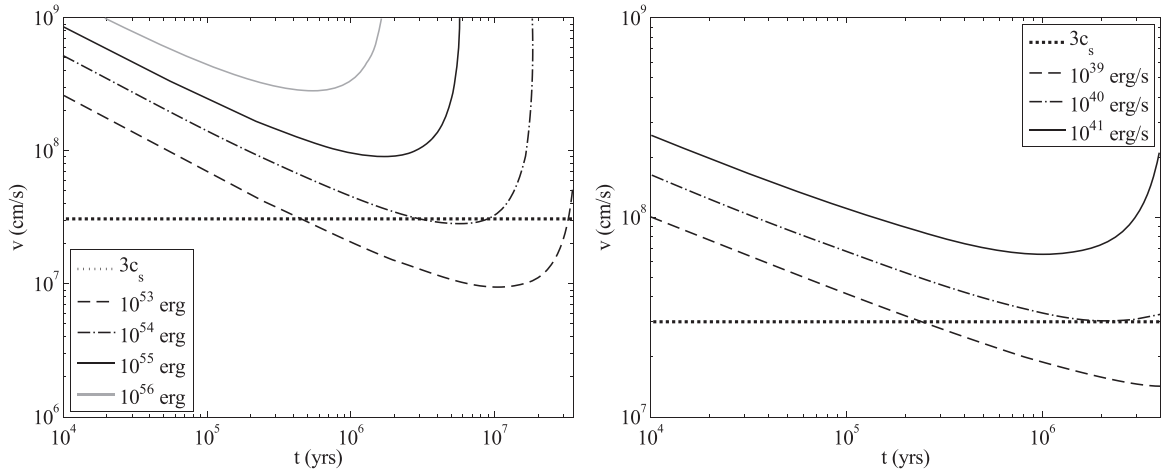

Figure 2. Temporal variation of the shock velocity of the top of the bubble for the case of the exponential halo with $z_0 = 0.67$ kpc and $n_0 = 0.03$ cm^{-3}. Left panel: one single input of energy at the GC. Right panel: multiple TDEs with different values of the power release in the GC. The horizontal dotted line indicates the velocity that is necessary for the shock not to stall in the halo. It is three times the sound speed in the halo 3×10^7 cm s^{-1}.

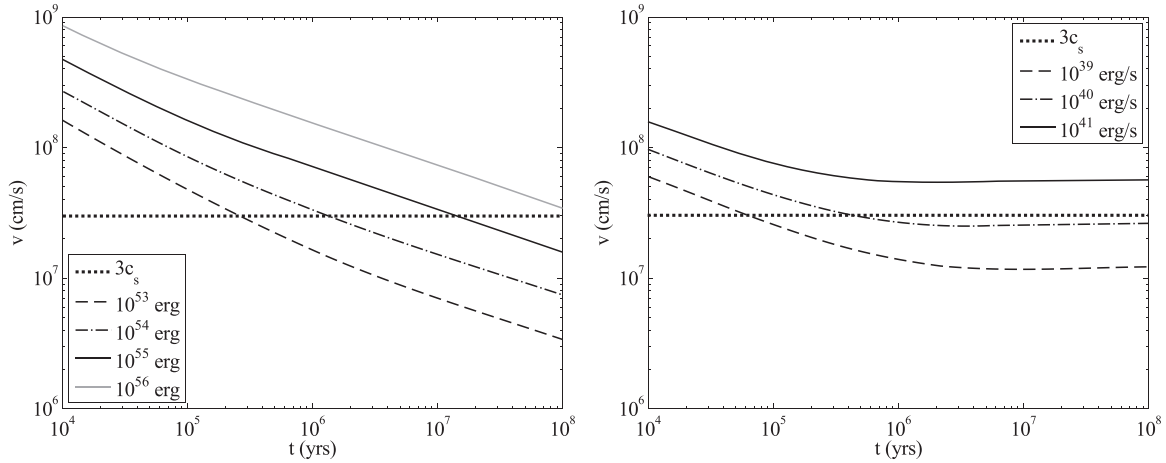

Figure 3. Same as Figure 2 except for a power-law halo with $z_c = 0.26$ kpc and $n_0 = 0.46$ cm^{-3}. Left panel: one single input of energy at the GC. Right panel: multiple TDEs with different values of the power release in the GC. The horizontal dotted line is three times the sound speed in the halo 3×10^7 cm s^{-1}.

5. Numerical Results

To consolidate the findings of Section 4 we perform hydrodynamic simulations of single and sequential multiple "explosions" in an atmosphere or a halo. An explosion refers to a burst of energy input representing the energy release of a TDE. We adopted the publicly available MHD simulation package FLASH (Fryxell et al. 2000, 2010). To reflect on the simple situation in Section 4, we keep only the minimal physics (and do not consider magnetic field, heating and cooling, etc.).

The background halo (or the initial condition for the halo) is an isothermal gas (i.e., pressure is proportional to density) in hydrostatic equilibrium (i.e., gravity is balanced by pressure gradient). We consider two types of density distributions: (1) exponential, see Equation (5), and (2) β-model, see Equation (7) (with $R = 0$). Once the density profile is known, the gravitational field required for hydrostatic equilibrium can be obtained. In fact, the sole purpose of the gravitational field here is to keep the unperturbed background in equilibrium; it does not affect the development of the bubbles as the thermal and kinetic energy of the bubble is much larger than the potential energy.

An explosion is implemented as an instantaneous energy release in the form of pure thermal energy uniformly distributed in a sphere of radius ~200 pc.

Figure 4 shows the density distribution of the bubble in an exponential halo. The temperature of the halo and the mass density at the midplane are taken as 10^6 K and 1.24×10^{-26} g cm^{-3}. The left panel shows the case of sequential multiple TDEs or explosions that each explosion releases 10^{53} erg and the interval between explosions is 0.01 Myr. This provides an average power (or luminosity) $\dot{W} = 3.3 \times 10^{41}$ erg s^{-1}. The simulation stops at 7.5 Myr as the bubble boundary approaches the edge of the simulation box. For comparison, in the right panel, we show the case of a single TDE or explosion. We take the energy release of this explosion to be 7.5×10^{55} erg, which is the same as the total energy release of the case of multiple explosions at the end of its simulation. However, in the single explosion case the expansion rate is higher, and the bubble is of comparable size (the top is $9 \sim 10$ kpc) at 4 Myr only.

Figure 5 shows the density distribution of the bubble in a β-model halo. The temperature of the halo and the density at the midplane are taken as 1.26×10^6 K and 9.50×10^{-25} g cm^{-3}, and the parameter $\beta = 0.71$ (Miller & Bregman 2013). The left panel shows the case of sequential multiple explosions that each explosion releases 10^{53} erg and the interval between explosions is 0.01 Myr. The simulation stops at 18 Myr. In the right panel, we show the case of a single explosion with the energy release

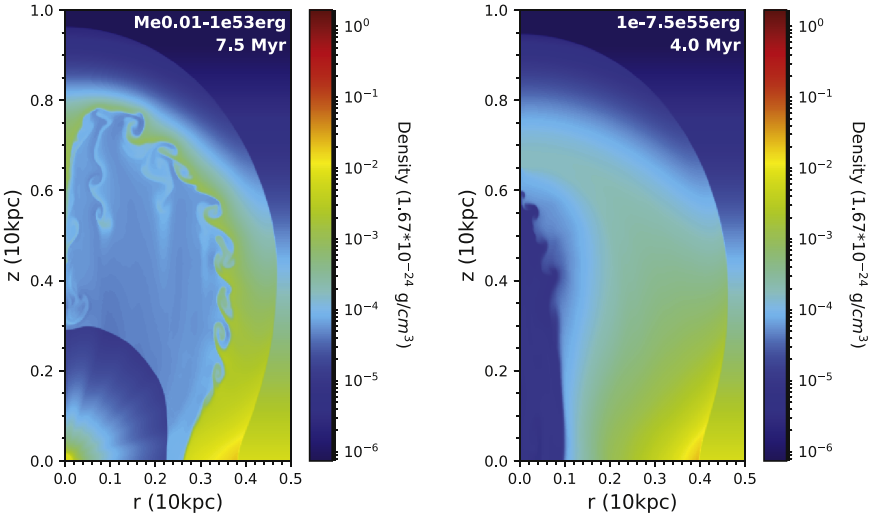

Figure 4. Numerical simulation of the Fermi Bubbles or similar structures in an exponential halo. The color maps in the figure show the density distribution in logarithmic scale. Left panel: multiple TDEs with each TDE releasing 10^{53} erg of energy and the interval between successive TDEs is 0.01 Myr; the simulation ends at 7.5 Myr. Right panel: single TDE with an energy release 7.5×10^{55} erg; the simulation ends at 4 Myr. The total energy released at the end of the simulations is the same for the two cases, i.e., 7.5×10^{55} erg.

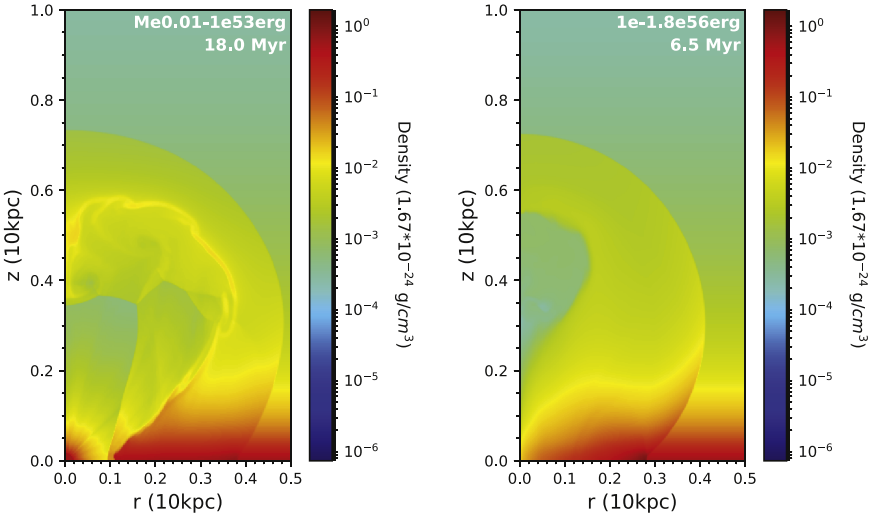

Figure 5. Same as Figure 4 except for a β-model halo. The color scale is the same as in Figure 4. Left panel: multiple TDEs with each TDE releasing 10^{53} erg of energy and the interval between successive TDEs is 0.01 Myr; the simulation ends at 18 Myr. Right panel: single TDE with an energy release of 1.8×10^{56} erg; the simulation ends at 6.5 Myr. The total energy released at the end of the simulations is the same for the two cases, i.e., 1.8×10^{56} erg.

1.8×10^{56} erg, which is the same as the total energy release of the case of multiple explosions at the end of its simulation. In the single explosion case the expansion rate is higher, we stop the simulation at 6.5 Myr when the bubble is of comparable size.

Comparing the two examples presented here, we note that it takes more time and energy for the bubble to develop in the β-model halo than the exponential halo. From Figures 4 and 5, we observed that the bubble envelope is more slender in an exponential halo while it is rounder in a β-model halo. (Note that the color scales of Figures 4 and 5 are the same.) These agree well with the analytical results in Section 4. Moreover, the interior of the bubble in the case of multiple explosions has a lot of shocks and is more turbulent for both halos. Thus, the routine explosions or routine TDE scenario is more conducive to particle acceleration.

6. Discussion and Conclusions

We have shown by analyzing the energy release from TDEs that it is possible to provide a sufficient amount of energy, even for a molecular cloud environment near the GC. The crucial point here is that the filling factor of molecular gas is sufficiently below unity, as is the case for the normal ISM. We have shown that density profiles following an exponential decay or a β-model in the lower halo cannot stall shocks in general. In addition, as we have shown, the ongoing energy input by TDEs resembles more that of a wind than a point explosion, which can drive the shock further out, as energy is constantly added to the bubble thus delaying catastrophic cooling by reheating, as has been shown by Kahn (1998) in the context of the Galactic fountain.

Here is a summary of our conclusions.

1. The standard interpretation of the FB origin is one huge energy release of about $10^{55} \sim 10^{56}$ erg in the GC (see, e.g., Su et al. 2010; Zubovas & Nayakshin 2012), whose envelope propagates through the Galactic halo. Our calculations show that, for the case of β-model halo density profile, the envelope disappears in the halo within

10^8 yr even for an energy as high as 10^{56} erg (see the left panel of Figure 3). For the case of the exponential density profile, the energy release must exceed 10^{54} erg in order for the envelope to penetrate into the halo (see the left panel of Figure 2).

2. Cheng et al. (2011) suggested a phenomenological model of FBs as a result of routine star disruptions by the supermassive black hole in the GC. They did not derive the model parameters quantitatively, but had a rough estimation of the energy release $\gtrsim 10^{53}$ erg. In our present analysis we concluded that the expected energy release is indeed about 10^{53} erg. Dai et al. (2018) showed that the accretion energy is mainly carried away by radiation (∼3%), a jet (∼20%), and hydrodynamic outflow (∼20%). The total energy of the outflow is about $10^{52} \sim 10^{53}$ erg, which is about 10% of the total rest mass energy of the disrupted star. In addition, if the X-ray chimney near GC (of energy $\sim 4 \times 10^{52}$ erg, Ponti et al. 2019) and radio bipolar bubbles near the GC (of energy $\sim 7 \times 10^{52}$ erg, Heywood et al. 2019) come from a TDE by the supermassive black hole at the GC, then it is consistent with our estimates concerning the energy release by TDEs.
3. The main concern is that the energy release for one TDE of 10^{53} erg is not high enough to penetrate through a medium of $50\,\mathrm{cm}^{-3}$ around the GC. However, routine star captures at a rate $\gtrsim 10^{-4}$ yr^{-1} resulting in an average energy luminosity at the GC of about $\dot{W} \sim 3 \times 10^{41}$ erg s^{-1} can enable a shock to penetrate through the disk into the halo and form the FBs or similar structures.
4. Another concern is that the gas of multicomponent distribution in the halo is not well known. We considered two models of gas distribution in the halo: exponential and beta-model. The evolution of the FB envelope (and similar structures) is quite different for the two models. For the exponential distribution the envelope propagates through the halo with acceleration. A stationary envelope structure is formed at a finite time (of the order of 10^7 yr), and the lateral radius of the envelope is about π times the scale height. Moreover, the top of the envelope may be destroyed by Rayleigh–Taylor instability (see Baumgartner & Breitschwerdt 2013).

   For the β-model halo, the envelope propagates through the halo with deceleration. In the limit, the velocity at the top is constant, and the envelope can extend to infinity in all directions.
5. Thus, we conclude that for routine TDEs at the GC, the bubble can exist for a long time ($>10^7$ yr) provided that $\dot{W} > 10^{40} \sim 10^{41}$ erg s^{-1} (see right panels of Figures 2 and 3).
6. Numerical simulations agree with the analytical solutions for both exponential and β-model halos. From the two examples we have in Section 5, it takes more energy and time for the bubble to develop in a β-model halo. Moreover, when comparing with the single huge energy release case, the interior of the bubble in the multiple TDEs' case is more turbulent and is more promising for cosmic-ray acceleration.
7. The presented hydrodynamic analysis may serve as a background model for acceleration processes in the FBs or similar structures.

The authors are grateful to Katia Ferrière, Miguel Avillez, and Takeshi Oka for fruitful discussions. C.M.K. and H.C. are supported in part by the Taiwan Ministry of Science and Technology grants MOST 105-2112-M-008-011-MY3, MOST 108-2112-M-008-006 and MOST 109-2112-M-008-005. D.O.C. and V.A.D. are supported by the grants RFBR 18-02-00075 and RSCF 20-12-00047. D.O.C. is supported in parts by foundation for the advancement of theoretical physics "BASIS." L.D. acknowledges support by the Danish National Research Foundation (DNRF132).

Software: FLASH (http://flash.uchicago.edu/site/flashcode/ Fryxell et al. 2000, 2010).

ORCID iDs

C. M. Ko https://orcid.org/0000-0002-6459-4763
D. O. Chernyshov https://orcid.org/0000-0003-0716-5951

References

Ackermann, M., Albert, A., Atwood, W. B., et al. 2014, ApJ, 793, 64
Akita, M., Kataoka, J., Arimoto, M., et al. 2018, ApJ, 862, 88
Alexander, T. 2005, PhR, 419, 65
Alexander, T., & Livio, M. 2004, ApJL, 606, L21
Avedisova, V. S. 1972, SvA, 15, 708
Baumgartner, V., & Breitschwerdt, D. 2013, A&A, 557, 140
Bisnovatyi-Kogan, G. S., & Silich, S. A. 1995, RvMP, 67, 661
Biswas, S., & Gupta, N. 2018, JCAP, 07, 063
Bland-Hawthorn, J., & Cohen, M. 2003, ApJ, 582, 246
Blondin, J. M., Wright, E. B., Borkowski, K. J., & Reynolds, S. P. 1998, ApJ, 500, 342
Breitschwerdt, D., McKenzie, J. F., & Völk, H. J. 1991, A&A, 245, 79
Burrows, D. N., Kennea, J. A., Ghisellini, G., et al. 2011, Natur, 476, 421
Carretti, E., Crocker, R. M., Staveley-Smith, L., et al. 2013, Natur, 493, 66
Cheng, K.-S., Chernyshov, D. O., & Dogiel, V. A. 2006, ApJ, 645, 1138
Cheng, K.-S., Chernyshov, D. O., & Dogiel, V. A. 2007, A&A, 473, 351
Cheng, K.-S., Chernyshov, D. O., Dogiel, V. A., et al. 2012, ApJ, 746, 116
Cheng, K.-S., Chernyshov, D. O., Dogiel, V. A., & Ko, C. M. 2014, ApJ, 790, 23
Cheng, K.-S., Chernyshov, D. O., Dogiel, V. A., & Ko, C. M. 2015, ApJ, 805, 135
Cheng, K.-S., Chernyshov, D. O., Dogiel, V. A., Ko, C. M., & Ip, W.-H. 2011, ApJL, 731, L17
Cordes, J. M., Weisberg, J. M., Frail, D. A., et al. 1991, Natur, 354, 121
Cox, D. P. 1972, ApJ, 178, 159
Crocker, R. M., & Aharonian, F. 2011, PhRvL, 106, 101102
Dai, L., McKinney, J. C., Roth, N., et al. 2018, ApJL, 859, L20
Dobler, G., Finkbeiner, D. P., Cholis, I., et al. 2010, ApJ, 717, 825
Donato, D., Cenko, S. B., Covino, S., et al. 2014, ApJ, 781, 59
Drury, L. O'C., & Völk, J. H. 1981, ApJ, 248, 344
Ferrière, K. 2001, RvMP, 73, 1031
Ferrière, K. 2012, A&A, 540, A50
Ferrière, K., Gillard, W., & Jean, P. 2007, A&A, 467, 611
Finkbeiner, D. P. 2004, ApJ, 614, 186
Fryxell, B., Olson, K., Ricker, P., et al. 2000, ApJS, 131, 273
Fryxell, B., Olson, K., Ricker, P., et al. 2010, FLASH: Adaptive mesh hydrodynamics code for modeling astrophysical thermonuclear flashes, v4.5, Astrophysics Source Code Library, ascl:1010.082
Gaensler, B. M., Madsen, G. J., Chatterjee, S., & Mao, S. A. 2008, PASA, 25, 184
Generozov, A., Stone, N. C., Metzger, B. D., & Ostriker, J. P. 2018, MNRAS, 478, 4030
Genzel, R., Eisenhauer, F., & Gillessen, S. 2010, RvMP, 82, 3121
Gillessen, S., Eisenhauer, F., Fritz, T. K., et al. 2009, ApJL, 707, L114
Guo, F., & Mathews, W. G. 2012, ApJ, 756, 181
Guo, F., Mathews, W. G., Dobler, G., & Oh, S. P. 2012, ApJ, 756, 182
Heywood, I., Camilo, F., Cotton, W. D., et al. 2019, Natur, 573, 235
Jew, L., & Grumitt, R. 2020, MNRAS, 495, 578
Jiang, Y.-F., Stone, J. M., & Davis, S. W. 2014, ApJ, 796, 106
Kahn, F. D. 1998, in The Local Bubble and Beyond, ed. D. Breitschwerdt et al., Vol. 506 (Berlin: Springer)
Kara, E., Miller, J. M., Reynolds, C., & Dai, L. 2016, Natur, 535, 388
Kataoka, J., Tahara, M., Totani, T., et al. 2015, ApJ, 807, 77
Kauffmann, J. 2017, arXiv:1712.01453

Keshet, U., & Gurwich, I. 2018, MNRAS, 480, 223
Kompaneets, A. S. 1960, DoSSR, 130, 5
Li, D., Saxton, R. D., & Yuan, W. 2020, ApJ, 891, 121
Li, J.-T., Hodges-Kluck, E., Stein, Y., et al. 2019, ApJ, 873, 27
Lin, D., Guillochon, J., Komossa, S., et al. 2017, NatAs, 1, 0033
Magorrian, J., & Tremaine, S. 1999, MNRAS, 309, 447
McCray, J., Weaver, R., & Castor, R. 1975, ApJL, 200, L107
McKee, C. F., & Ostriker, J. P. 1977, ApJ, 218, 148
Melia, F., & Falcke, H. 2001, ARA&A, 39, 309
Mertsch, P., & Sarkar, S. 2011, PhRvL, 107, 091101
Miller, M. J., & Bregman, J. N. 2013, ApJ, 770, 118
Miller, M. J., & Bregman, J. N. 2016, ApJ, 829, 9
Mills, E. A. C. 2017, arXiv:1705.05332
Mills, E. A. C., Ginsburg, A., Immer, K., et al. 2018, ApJ, 868, 7
Morris, M., Baganoff, F., Muno, M., et al. 2003, ANS, 324, 167
Morris, M., & Serabyn, E. 1996, ARA&A, 34, 645
Mou, G., Yuan, F., Bu, D., et al. 2014, ApJ, 790, 109
Nakashima, S., Inoue, Y., Yamasaki, N., et al. 2018, ApJ, 862, 34
Nakashima, S., Koyama, K., Wang, Q. D., et al. 2019, ApJ, 875, 32
Nayakshin, S., & Zubovas, K. 2018, MNRAS, 478, L127
Nogueras-Lara, F., Schödel, R., Gallego-Calvente, A. T., et al. 2020, NatAs, 4, 377
Nordgren, T. E., Cordes, J. M., & Terzian, Y. 1992, AJ, 104, 1465
Oka, T., Geballe, Th. R., Goto, M., et al. 2019, ApJ, 883, 54
Planck Collaboration IX 2013, A&A, 554, A139
Ponti, G., Hofmann, F., Churazov, E., et al. 2019, Natur, 567, 347
Rubtsov, G., & Zhezher, Y. 2018, arXiv:1812.05228
Sądowski, A., & Narayan, R. 2016, MNRAS, 456, 3929
Sedov, L. I. 1959, Similarity and Dimensional Methods in Mechanics (New York: Academic)
Shapiro, P. R. 1979, ApJ, 233, 831
Snowden, S. L., Egger, R., Freyberg, M. J., et al. 1997, ApJ, 485, 125
Su, M., Slatyer, T. R., & Finkbeiner, D. P. 2010, ApJ, 724, 1044
Syer, D., & Ulmer, A. 1999, MNRAS, 306, 35
Tahara, M., Kataoka, J., Takeuchi, Y., et al. 2015, ApJ, 802, 91
Totani, T. 2006, PASJ, 58, 965
Wang, J., & Merritt, D. 2004, ApJ, 600, 149
Weaver, R., McCray, R., Castor, J., et al. 1977, ApJ, 218, 377
Yang, H.-Y., Ruszkowski, M., & Zweibel, E. 2018, Galax, 6, 29
Yang, H.-Y. K., Ruszkowski, M., Ricker, P. M., Zweibel, E., & Lee, D. 2012, ApJ, 761, 185
Zel'dovich, Ya. B., & Raizer, Yu. P. 1967, Physics of Shock Waves and High-Temperature Hydrodynamic Phenomena (New York: Academic)
Zhang, R., & Guo, F. 2020, ApJ, 894, 117
Zhang, Z., Murase, K., & Mészáros, P. 2020, MNRAS, 492, 2550
Zhao, J.-H., Morris, M. R., & Goss, W. M. 2016, ApJ, 817, 171
Zubovas, K., King, A. R., & Nayakshin, S. 2011, MNRAS, 415, L21
Zubovas, K., & Nayakshin, S. 2012, MNRAS, 424, 666